Applied Catalysis B: Environmental 100 (2010) 102–115

Contents lists available at ScienceDirect

Applied Catalysis B: Environmental

journal homepage: www.elsevier.com/locate/apcatb

Effect of the support on activity of silver catalysts for the selective reduction of NO by propene

N. Hickey[a,b,*], I. Boscarato[a,b], J. Kašpar[a,b], L. Bertinetti[c], M. Botavina[c], G. Martra[c]

[a] Dipartimento di Scienze Chimiche, Università di Trieste, Via Giorgieri 1, I-34127 Trieste, Italy
[b] INCA – Interuniversity Consortium "Chemistry for the Environment", Research Unit Trieste 1, Italy
[c] Dipartimento di Chimica IFM & Interdipartimental NIS Center of Excellence – Università di Torino, Via P. Giuria 7, I-10125 Torino, Italy

ARTICLE INFO

Article history:
Received 14 April 2010
Received in revised form 7 July 2010
Accepted 16 July 2010
Available online 22 July 2010

Keywords:
Ag catalysts
Ceria–zirconia
Zirconia
Alumina
SO_2

ABSTRACT

Use of zirconia, ceria–zirconia and ceria supports for Ag-based lean deNO_x catalysts lowers the temperature range of activity by about 150–200 K with respect to Al_2O_3-supported analogues. *Ex situ* characterisation of the catalysts indicates that this remarkable effect is associated with a role of the support rather than Ag dispersion. The crucial role of the support is further evidenced by suppression of CO formation over these catalysts and by significant support-related differences when SO_2 is added to the feed. The presence of ceria in the formulation results in an initial resistance to the deactivating effect of SO_2; while the use of both zirconia and ceria–zirconia facilitates reactivation after sulphur poisoning.

1. Introduction

Following the initial report by Miyadera and Yoshida [1] that Ag/Al_2O_3 exhibits high activity and selectivity to N_2 production, this catalyst has received considerable attention as a candidate for the direct selective catalytic reduction (SCR) of NO_x by hydrocarbons and oxygenates in automotive exhaust streams. CH_4, C_3H_6, C_3H_8, mixtures of C_3H_6 and C_3H_8, gasoline, diesel fuel, higher hydrocarbons, CH_3OH, C_2H_5OH and $(CH_3)_2CO$ have all been investigated as reducing agents [2–5].

For simplicity, the activity characteristics of C_3H_6-SCR over Ag/Al_2O_3 catalysts may be divided into two regimes: at lower Ag loading they show a maximum of deNO_x activity around 773 K, with very high selectivity to N_2; while at higher Ag loading (>6%) the maximum of NO_x conversion is at lower temperature and selectivity towards N_2O and NO_2 increases. The changes observed upon increasing the loading have been attributed to a change in mechanism: at high Ag content the low temperature activity was attributed to the presence of large metallic particles under reaction conditions, with a mechanism similar to that reported over Pt/Al_2O_3; while at lower Ag content the activity was attributed to more dispersed Ag particles, which are maintained oxidised by the support [6,7]. An optimal Ag loading, which varies according to the surface area of the catalyst, has been widely reported. The presence of large Ag particles was also suggested for a decrease in the temperature of NO_x conversion over Ag/ZrO_2 compared to Ag/Al_2O_3 as the Ag loading was increased from 0.2% to 2% [7]. Haneda et al. reported a similar effect of Ag loading for Ag/TiO_2–ZrO_2 [8]. The very high surface area of their sample (284 $m^2\,g^{-1}$) should not have favoured the formation of large particles however. We have reported that the use of zirconia-based supports promotes low temperature deNO_x activity relative to Ag/Al_2O_3 [9]. This observation is of particular interest in the context of the so-called hydrogen effect, in which a dramatic improvement in the low temperature deNO_x activity is observed upon introduction of small amounts of hydrogen to the feed when alumina and some zeolites are used as the support, but not when TiO_2, ZrO_2 or SiO_2 are used [3]. It is important to underline that, irrespective of the mechanism of promotion, low temperature deNO_x activity is a highly desirable characteristic.

The effect of SO_2 and H_2O on activity is of fundamental importance for any potential deNO_x catalyst. It appears clear from the reports in the scientific literature that the H_2O- and SO_2-tolerance of Ag-based catalysts is dependent on many factors (Ag loading, preparation method, reductant used, etc.) and the exact behaviour observed is specific to the catalyst/reaction system investigated. With regard to SO_2, there is much evidence to suggest that it is a poison for HC deNO_x activity under lean conditions, although SO_2-induced promotion has also been reported [10,11]. Oxygenated

* Corresponding author at: Dipartimento di Scienze Chimiche, Università di Trieste, Via Giorgieri 1, I-34127 Trieste, Italy. Tel.: +39 040 558 3977; fax: +39 040 558 3903.
E-mail address: nhickey@units.it (N. Hickey).

0926-3373/$ – see front matter © 2010 Elsevier B.V. All rights reserved.
doi:10.1016/j.apcatb.2010.07.019

molecules show a higher resistance to the deactivating effect of SO_2. Satokawa et al. have reported appreciable on-stream deactivation for the selective reduction of NO by C_3H_8 over 2% Ag/Al_2O_3 at SO_2 concentrations as low as 0.5 ppm [12]. Such deactivation is invariably attributed to the accumulation of sulphate species on both silver and aluminium and the deactivation–regeneration behaviour is therefore strongly dependent on reaction temperature. Using C_3H_8 as reductant, Satokawa et al. have shown that the deactivation observed is less pronounced at 823 K as compared to 723 or 773 K, while Meunier et al. [13] have shown that severe procedures, which can lead to metal sintering, are required to regenerate activity of a sulphated 1.2% Ag/Al_2O_3 material for C_3H_6-SCR: neither thermal treatment at 1123 K nor reduction (10% H_2) at 1023 K fully restore the activity after *ex situ* sulphation at 759 K.

With respect to a dry feed, activity of Ag/Al_2O_3 in the presence of water vapour is strongly dependent on the reducing agent. With short chain hydrocarbons (usually C3), investigations almost exclusively indicate that there is deactivation [1,7,14], which is reversible upon removal of H_2O from the feed stream [7,15]. Shimizu et al. [16] have reported that with longer chain hydrocarbons there is either deactivation (n-hexane) or activity promotion (n-octane) in the presence of H_2O, the extent of which is dependent on H_2O concentration. Possible explanations offered for the promotional effect were the inhibition of unselective oxidation and the suppression of poisoning by carbonaceous deposits. When oxygenates are used as reducing agents, the evidence suggests that relatively high activity is maintained. These observations have lead to the suggestion that the negative effect of water is due to adsorption competition, with oxygenated molecules better able to compete with water than light hydrocarbons [7].

Finally, the combined effect of the presence of SO_2 and H_2O under reaction conditions is another important consideration. In fact, one of the more notable features of the Ag/Al_2O_3 catalyst reported by Miyadera and Yoshida [1] is that the deNO_x activity at 673 K was higher in the presence of both SO_2 and H_2O than in the presence of H_2O only, although activity was highest in a dry, SO_2-free feed. In line with this, the majority of reports conclude that catalysts are poisoned in the presence of SO_2 and H_2O.

Here, we present an investigation of the effects of the support and of Ag dispersion on the activity of various Ag catalysts; as well as an investigation of their activity in the presence of SO_2 and H_2O.

2. Experimental

Two types of γ-Al_2O_3 were employed: a commercial sample (ALFA 100 $m^2\,g^{-1}$) and a previously described high surface area material (180 $m^2\,g^{-1}$) [17]. $Ce_{0.16}Zr_{0.84}O_2$ solid solution was prepared by co-precipitation of a solution containing cerium nitrate and zirconium nitrate mixed in appropriate quantities [18], while ZrO_2 samples (100 and 40 $m^2\,g^{-1}$) were prepared by precipitation of solutions containing zirconium nitrate. After precipitation, the resulting hydroxide materials were washed with water, dried overnight at 393 K and calcined at 973 K for 5 h. CeO_2 and $Ce_{0.2}Zr_{0.8}O_2$ were supplied by RHODIA and MEL Chemicals, respectively. To vary the final dispersions obtained, Ag (2 wt% in all cases) was loaded by either incipient wetness (IW) or depositing a preformed Ag sol (SOL) onto the support [19], using $AgNO_3$ as precursor in both methods. After deposition, the materials were dried overnight at 353 K and calcined at 923 K for 5 h. A reference 1% Pt/Al_2O_3 sample was prepared by IW, using the high surface area Al_2O_3 support and hexachloroplatinic acid as the precursor.

Full activity profiles were obtained by increasing the temperature in steps of 25 K and monitoring activity for 40–90 min at each temperature. Analysis was performed by gas chromatography using Molecular Sieve and Poraplot Q columns (C_3H_6, CO_2, CO, O_2, N_2O, N_2) and an Eco Physics CDL700 chemiluminescence detector (NO, NO_2, total-NO_x). The nitrogen balance was within 3% in all measurements. Temperature programmed reaction profiles were recorded by heating the sample in the reaction mixture from room temperature (rt) to 873 K at 10 K min^{-1}. Isothermal activity profiles were obtained by passing the reaction mixture over the sample at the selected temperature, after heating to that temperature in He flow at a heating rate 10 K min^{-1}. Samples were subjected to a cleaning procedure using 5% O_2 in He at 923 K for 1 h before all activity tests or set of activity tests. The reaction mixture typically contained 1000 ppm NO, 1000 ppm C_3H_6, 5% O_2 and, when present, 50 ppm SO_2 and/or 10 vol% H_2O (balance He), with a weight/flow rate ratio (W/F) of 0.05 g_{cat} s ml^{-1} (50 mg of catalyst, 60 ml min^{-1}). It should be noted that the NO source contained an NO_2 impurity at a concentration of 1% of the NO concentration. This has been taken into consideration in the data reported. A number of activity tests were performed after *ex situ* treatments of the samples in a mixture of 50 ppm SO_2 + 5% O_2 (60 ml min^{-1}). After this treatment, the samples were transferred in air to perform the activity tests. Regeneration of sulphated samples at various temperatures was performed with a mixture containing 5% H_2 in He. Details of all conditions used are specified in the relevant text and figure captions.

Two types of temperature programmed reduction (TPR) profiles were measured: (1) the sample (200 mg) was first treated in a mixture of 300 ppm SO_2 + 5% O_2 at rt (balance He), before the temperature was raised to 873 K, held for 1 h and then cooled slowly to rt. These conditions ensure significant sulphur uptake. 5% H_2 in He was then passed over the sample and the temperature was raised (10 K min^{-1}) to 873 K; (2) the sample was treated in 300 ppm SO_2 + 5% O_2 (balance He) for 1 h at 723 K before switching to 5% H_2 in He. After a period of isothermal treatment, the temperature was raised (10 K min^{-1}) to 1073 K. The signals for SO_2 and H_2S were monitored in the reducing atmosphere using a quadrupole mass spectrometer (QMS) detector. Flow rates were 25 ml min^{-1}.

Specific surface areas (BET method, SSA_{BET}) were measured using a Micromeritics ASAP analyser using N_2 at 77 K.

Transmission electron microscopy (TEM) measurements were carried out on a Jeol 2010F instrument, equipped with an EDS system for elemental analysis (probe size under 0.5 nm). A small amount of sample was ultrasonically dispersed in isopropyl alcohol and deposited on a copper grid covered with a lacey carbon film. Histograms of the particle size distribution were obtained by considering at least 300 particles on the TEM images, and the mean particle diameter (d_m) was calculated as $d_m = \Sigma d_i n_i / \Sigma n_i$, where n_i was the number of particles of diameter d_i. In some cases where the number of observable particles was well below 300, the limit values of the size measure were simply reported. The "theoretical" specific surface area of supported metal particles (supposed to be spherical) was calculated by the formula: $SSA = 3\Sigma n_i r_i^2 / (\rho_{Ag} \Sigma n_i r_i^3)$ m^2/g, where r_i was the mean radius of the size class containing n_i particles, and ρ_{Ag} the volumetric mass of Ag (10.5 g/cm^3). The theoretical metal area present in 1 g of catalyst was then calculated on the basis of the Ag loading.

3. Results

3.1. Catalyst characterisation

Table 1 summarises the samples prepared and investigated. SSA_{BET} of the catalysts are also reported. The final column contains the designations of the samples used throughout the text. Detection of Ag dispersion by chemisorption was attempted on the CeO_2-containing systems but, due to adsorption over the support, reliable data could not be obtained. TEM was therefore employed to

Table 1
Ag-based catalysts prepared and investigated.

Sample composition	Preparation method[a]	SSA_{BET} surface area ($m^2\ g^{-1}$)	Sample designation
2% $Ag/Ce_{0.16}Zr_{0.84}\ O_2$	IW	100	AgCeZr-1
	SOL	100	AgCeZr-2
2% Ag/ZrO_2	IW	40	AgZr-1
2% Ag/ZrO_2	IW	100	AgZr-2
2% Ag/Al_2O_3	IW	100	AgAl-1
		180	AgAl-2
2% Ag/CeO_2	IW	100	AgCe-1

[a] See Section 2 for details of preparation methods.

obtain indications on the silver dispersion in the different catalysts. In Table 2 the size range of Ag particles observed for each sample is reported, ranging from the domain of a few nm in the cases of AgZr-1, AgZr-2, AgCe-1, or even smaller in the case of AgCeZr-1, to the domain of a few tens of nm (AgCeZr-2). Four samples exhibited a high enough number of observable Ag particles (representative TEM images in Fig. 1) to allow a statistically meaningful analysis of the metal particles size and the results are reported in Fig. 2. Because the AgAl-1 sample exhibited a bimodal particle size distribution, two types of data have been calculated (i) the percentage number at each particle size; and (ii) the percentage mass at each particle size, assuming, for the purposes of the calculation, a spherical particle geometry. Furthermore, on the basis of the histogram at point (i) the metal specific surface area and the metal area present in 1 g of catalysts were calculated (Table 2). In both Ag/Al_2O_3 catalysts silver particles with size in the 3.0–20.0 nm were present, but in the case of AgAl-1 they contained only a minor part of the silver mass, the rest corresponding to much larger Ag particles (25–50 nm in size), the formation of which is likely a result of the lower specific surface area of the support. Finally, the metal particle size distribution obtained for the AgCeZr-2, resulting from the deposition of the support of a preformed Ag sol, appeared quite narrow.

3.2. Effect of the support on the SCR of NO over Ag catalysts

The main operational parameters and results of the $deNO_x$ activity tests carried out on the various catalysts are listed in Table 3. Due to the different reaction conditions, in particular space velocities, comparison of catalytic results with literature data is often difficult [20]. Accordingly, the activity of the Ag/Al_2O_3 catalysts are reported here mainly as reference catalysts under identical reaction conditions. For the sake of clarity, the discussion of $deNO_x$ activity for the Ag/Al_2O_3 catalysts will be presented separately from that of the others. Comparative results dealing with other features of the reaction using selected supports will then be presented.

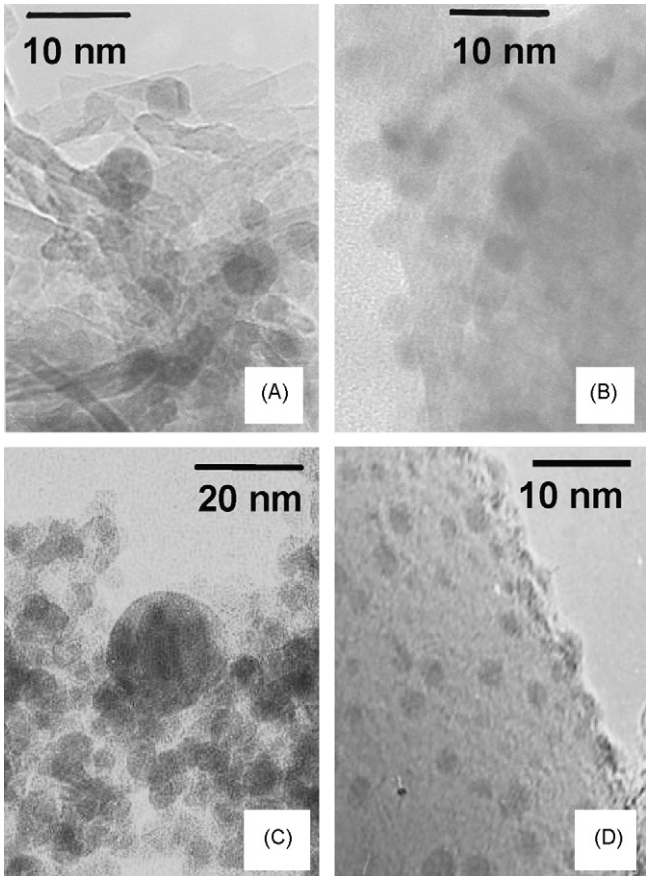

Fig. 1. Representative TEM images of: (A) AgAl-1, (B) AgAl-2, (C) AgCeZr-2, and (D) AgZr-1 catalysts.

3.2.1. Activity of Ag/Al_2O_3 catalysts

Fig. 3 contains a comparison of the most important features of the lean-$deNO_x$ activity of AgAl-1 and AgAl-2. Conversions of NO_x and C_3H_6 and selectivity to CO_2 and CO are shown. Both samples exhibit a maximum of NO_x conversion near 773 K, with very low NO conversion to NO_2 and N_2O (<3% of the NO feed, not shown). Thus, by mass balance, the NO_x conversion corresponds closely to NO conversion to N_2. C_3H_6 conversion reaches 100% at a temperature marginally above the $deNO_x$ maximum (80–90% at NO_x conversion maximum). Both materials show conversion of the hydrocarbon to CO. In general therefore, the overall characteristics of the data obtained over these catalysts are comparable to literature reports for similar materials. A somewhat unexpected feature, however, is the observation of a low temperature "plateau" in the C_3H_6 con-

Table 2
Ag particle size distribution of the catalysts.

Sample	Limits of the size distributions (average Ag particle size) (nm)	Metal specific surface area[a] ($m^2_{Ag}\ g^{-1}_{Ag}$)	Metal area in 1 g of catalyst[a] ($m^2_{Ag}\ g^{-1}_{cat}$)
AgCeZr-1	See note[b]	>155[e]	>3.10[e]
AgCeZr-2	20.0–30.0 (25.0)	23	0.46
AgZr-1	1.5–6.5 (4.0)	155	3.10
AgZr-2	1.5–3.5[c]	>155[e]	>3.10[e]
AgAl-1	4.0–15.0 (8.0); 27.0–50.0[d]	23	0.46
AgAl-2	3.5–18.5 (11.0)	48	0.96
AgCe-1	0.5–2.0[c]	>155[e]	>3.10[e]

[a] Calculated assuming a spherical particle geometry.
[b] Due to poor contrast with the support, no Ag particles could be detected at the various magnifications employed. The presence of Ag was analytically detected by the TEM/EDS technique, which suggests that Ag should be dispersed with particles <1 nm.
[c] Due to poor contrast with the support and the very small size of particles, very few particles have been observed; the numbers reported in the table are based on the observation of about 30–40 particles in the case of AgZr-2 and 10–15 for in the case of AgCe-1.
[d] Bimodal particle distribution observed with about 80 mass% of the particles above 20 nm.
[e] Assumed to be larger than for the catalyst with the smallest Ag particles observable by TEM.

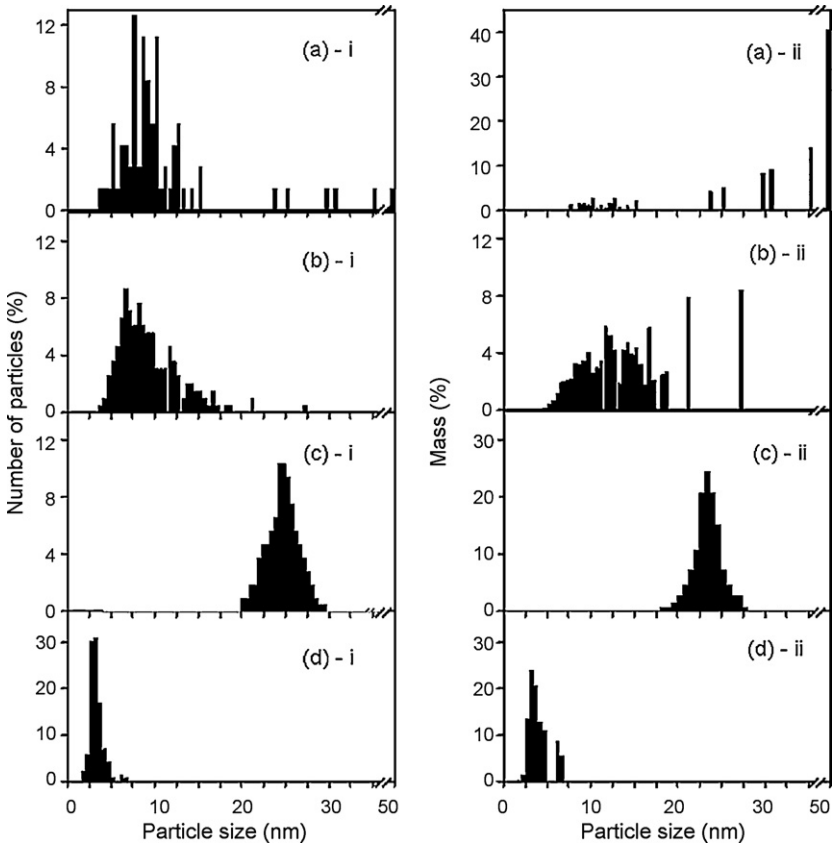

Fig. 2. Particle size distribution – as the percentage number (i) and percentage mass (ii) at each particle size – for selected Ag samples: (a) AgAl-1, (b) AgAl-2, (c) AgCeZr-2, (d) AgZr-1. The percentage mass was calculated assuming spherical particles. Histograms of the particle size distribution were obtained by considering at least 300 particles on the TEM images.

version for AgAl-1. A similar feature is present in the corresponding CO_2 formation curve, indicating that it may be attributed to unselective combustion, which in turn may be attributed to the Ag particle size distribution of this material (vide infra).

3.2.2. Activity of Ag catalysts supported on $Ce_{0.16}Zr_{0.84}O_2$, CeO_2 and ZrO_2

Figs. 4 and 5 summarise the deNO$_x$ activity of AgCeZr-1, AgCeZr-2, AgCe-1 and AgZr-1. For comparison, profiles of the direct C_3H_6 and NO oxidation reactions over AgCeZr-2 under identical reaction conditions are included in Fig. 4. Different extents of conversion at the maxima of deNO$_x$ activity are observed. However, all catalysts exhibit activity across a relatively low temperature range. As the maximum of NO$_x$ conversion is expected to strongly depend on the combustion activity, this observation is consistent with an enhanced combustion activity introduced by the presence of Ce and/or Zr in the catalyst formulations, i.e., an effect of the support. For the present samples, the NO$_x$ conversion maxima

Table 3
DeNO$_x$ activity of the various catalysts tested.

Sample	deNO$_x$ Activity[a]							
	Activity range[b] (K)	T_{10}[c] (K)	Maximum of deNO$_x$ activity[d]					
			T_{max} (K)	NO$_x$ conversion (%)	NO conversion to NO$_2$ (%)	NO conversion to N$_2$O[c] (%)	deNO$_x$ rate at 723 K[e]	
							$(mol\,s^{-1}\,g^{-1}) \times 10^7$	$(mol\,s^{-1}\,m^{-2}_{Ag}) \times 10^7$
AgCeZr-1	583–758	600	648	14	0	9	1.3	< 0.4
AgCeZr-2[f]	563–753	540	627 (729)	39 (29)	0 (2)	8 (4)	3.5	7.6
AgZr-1	578–738	555	648	36	11	11	3.2	1.3
AgZr-2[g]	580–729	543	645	39	2	-	3.4	<1.1
AgAl-1	718–868	685	798	37	0	1	3.3	7.2
AgAl-2	703–893	665	773	51	0	1	4.6	4.8
AgCe-1	523–733	550	631	14	3	6	1.2	<0.4

[a] 1000 ppm NO and C_3H_6, 5% O_2. W/F = 0.05 g s ml^{-1} in all cases.
[b] Temperature range where NO$_x$ conversion > 50% of maximum of NO$_x$ conversion.
[c] Light-off temperature. Defined as the temperature at which 10% NO$_x$ conversion is observed.
[d] All conversions refer to values at maximum and are calculated on the basis of the NO fed. NO$_x$ = NO + NO$_2$. Thus, any NO converted to NO$_2$ makes no contribution to NO$_x$ conversion.
[e] For comparison, values of 3.1×10^{-7} mol NO$_{x\ converted}$ g^{-1} s^{-1} at 713 K and 2.5×10^{-7} mol NO$_{x\ converted}$ g^{-1} s^{-1} at 723 K for 2% Ag/Al_2O_3, calculated from the data reported in Refs. [7,6]. Values in the last column were calculated by using data in the last column in Table 2.
[f] A high temperature shoulder was observed in NO$_x$ conversion. Data in parenthesis.
[g] Activity was measured under ramped conditions (10 K min^{-1}) and N$_2$O was not recorded. Data given for ramp-down.

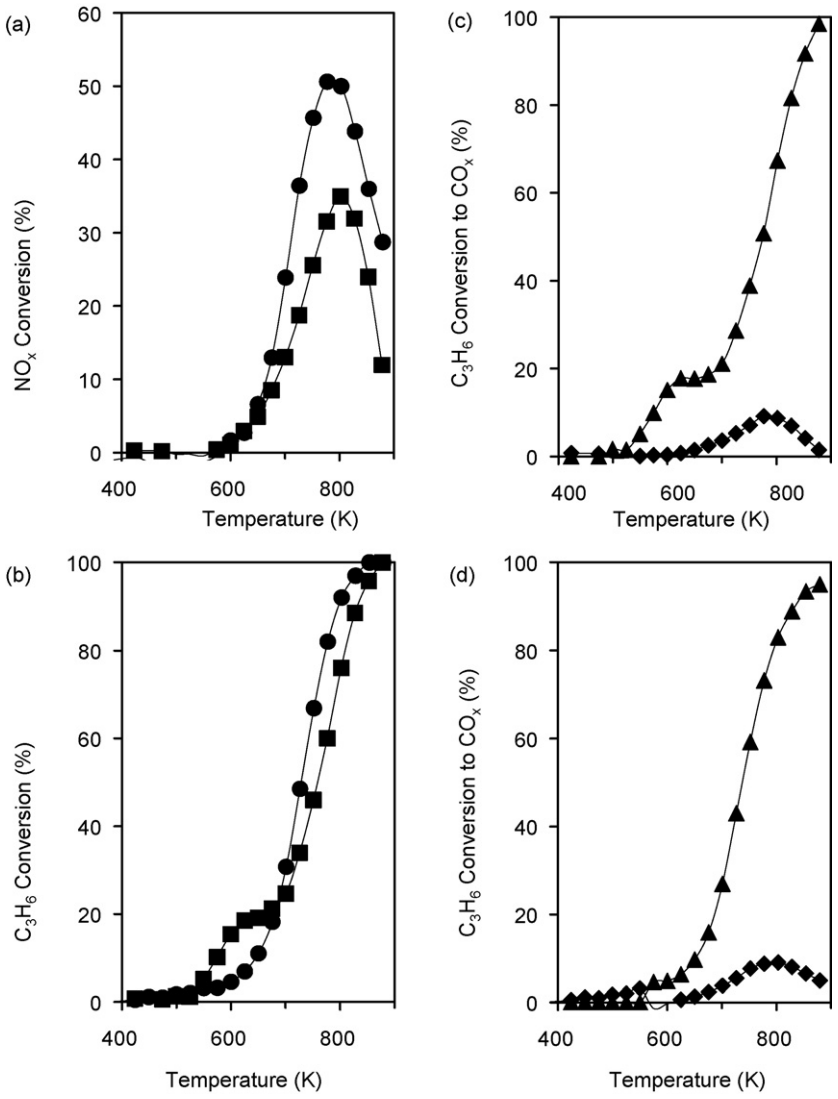

Fig. 3. Comparison of deNO_x activity of AgAl-1 and AgAl-2 as a function of temperature: (a) NO_x ($NO + NO_2$) and (b) C_3H_6 conversion over AgAl-1 (■) and AgAl-2 (●); Percentage of C_3H_6 converted to CO_2 (▲) and CO (♦) over (c) AgAl-1 and (d) AgAl-2. 1000 ppm NO, C_3H_6, 5% O_2. W/F = 0.05 g s ml^{-1}.

(Figs. 4a and 5a) are ca. 150 K below those shown in Fig. 3a for the Al_2O_3-based catalysts. Indeed, the temperature of initial activity of these materials is comparable with that of Pt/Al_2O_3 [21], albeit with significantly more gradual light-off, thereby resulting in an activity window (where NO_x conversion > 50% of maximum conversion) about 170 K wide. For comparison, the width of the deNO_x activity windows over Pt/Al_2O_3 catalysts is about 130 K at most [21]. The maximum in NO_x conversion for the present samples is however at higher temperature by ca. 90 K with respect to that normally observed for Pt/Al_2O_3 (see Fig. 14). Analogous relationships between the relative positions of maximum NO_x conversion and 100% C_3H_6 conversion are observed in Figs. 3–5, while the high temperature shoulder in NO_x conversion observed over AgCeZr-2 at ca. 725 K corresponds to the maximum of direct NO oxidation activity for this material (Fig. 4a). Significantly, no CO formation was detected for any of the catalysts in Figs. 4 and 5.

Figs. 4 and 5 indicate undesirable production of NO_2 and N_2O. For the zirconia-containing samples: AgCeZr-1 exhibits a maximum of 9% conversion of the NO feed to NO_2 and 7% to N_2O; for AgCeZr-2, maxima of 9% NO conversion to both NO_2 and N_2O are observed; while for AgZr-1, maxima of 18 and 12% NO conversion to NO_2 and N_2O are observed, respectively. The differences in selectivity are largely responsible for the marginally higher NO_x conversion of AgCeZr-2 (Fig. 4a). In fact, the total NO conversion is considerably higher for AgZr-1, but its higher selectivity towards NO_2 results in lower overall NO_x conversion. AgCe-1, investigated mainly to discriminate the effects of CeO_2 on the catalytic properties of the Ag/CeO_2–ZrO_2 systems, features rather low deNO_x activity and comparatively high NO_2 formation (26%), which could be associated with the high oxidation capability of this support. However, the activity range is the same as the Zr-containing samples.

Further tests (not shown) on a series of 2% $Ag/Ce_{0.16}Zr_{0.84}O_2$ and 2% $Ag/Ce_{0.2}Zr_{0.8}O_2$ catalysts confirm this lower temperature activity window in comparison with Ag/Al_2O_3, with differences observed only in the extent of conversion and selectivity.

The light-off behaviour for the catalysts is indicated in Table 3 by T_{10} values, i.e., the temperature at which 10% NO_x conversion is observed. These indicate a strong shift in light-off with respect to Al_2O_3 in the case of the other supports. The final column of Table 3 contains a comparison of the deNO_x rate, normalised to the Ag surface area per gram of catalyst. These data strongly indicate a decrease in rate with increasing dispersion.

The effect of space velocity was also investigated under ramp-up temperature programmed reaction conditions (10 K min^{-1}) over the AgAl-1 and AgCeZr-2 catalysts (data not shown). Under these conditions the behaviour was dominated, respectively, by NO_x des-

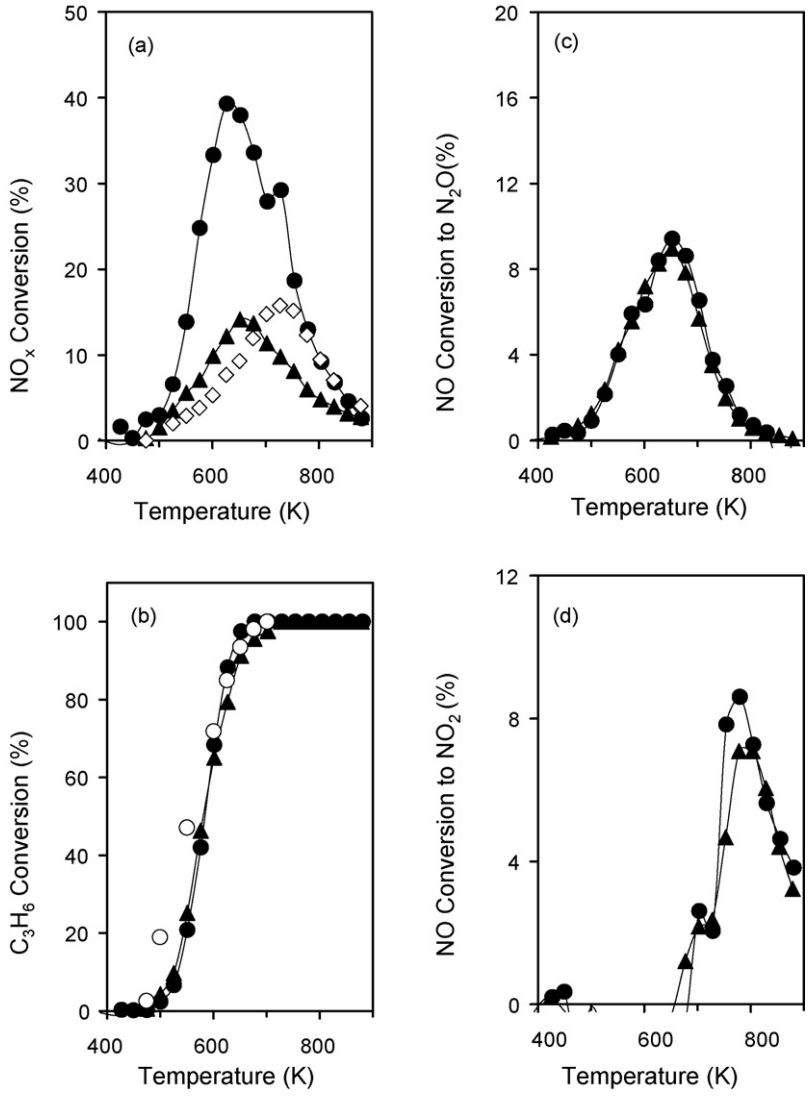

Fig. 4. Comparison of deNO_x activity of AgCeZr-1 (▲) and AgCeZr-2 (●) as a function of temperature: (a) NO_x (NO + NO_2) conversion, (b) C_3H_6 conversion, (c) NO conversion to N_2O, and (d) NO conversion to NO_2. 1000 ppm NO, C_3H_6, 5% O_2. W/F = 0.05 g s ml^{-1}. (◊) NO oxidation (1000 ppm NO, 5% O_2) and (○) C_3H_6 oxidation (1000 ppm C_3H_6, 5% O_2) over AgCeZr-2 under identical conditions of W/F.

orption (a mixture of NO and NO_2) at 300–600 and 300–500 K and NO_x conversion centred at 750–800 and 600–650 K. With regard to the NO_x conversion, altering the W/F by a factor of 4 (0.1–0.025 g s ml^{-1}) did not significantly change the activity ranges, while variation in the extent of conversion at maximum was observed. Comparison between ramped and steady state reaction under the same W/F conditions indicate almost identical activity ranges, with the activity at maximum slightly lower under temperature programmed reaction conditions, thereby indicating that the ramped method used does not significantly influence the result. Therefore, within the range used, space velocity does not determine the activity ranges of these samples.

3.3. The effect of SO_2 on the SCR of NO with C_3H_6

The effect of the support on sulphur tolerance was investigated over three representative samples: AgAl-1, AgCeZr-2 and AgZr-1. These samples not only show comparable maximum deNO_x conversions, but they also exhibit comparable conversions at 723 K, which facilitates direct comparison of the deactivation behaviour. In addition to the fact that sulphur tolerance is an important aspect of the catalytic behaviour, SO_2 adsorption offers the possibility to selectively poison the catalysts. The effect of SO_2 was investigated using a combination of both *in situ* and *ex situ* approaches. An investigation of the ability of H_2 to regenerate the catalysts by removal of adsorbed sulphate species was first conducted.

3.3.1. TPR after treatment with $SO_2 + O_2$

Fig. 6 shows the removal of sulphur species during TPR from AgAl-1, AgCeZr-2 and Ag Zr-1 after treatment of the fresh samples with $SO_2 + O_2$. Normalisation of the integrated signals to the surface areas of the samples indicated that the least amount of sulphur species is removed from AgAl-1. Both H_2S and SO_2 desorb, indicating the presence of different types of surface sulphates [22]. Like AgAl-1, a mixture of H_2S (1.5 times the amount observed from AgAl-1/m^2) and SO_2 (3.4 times the amount observed from AgAl-1/m^2) is removed from AgCeZr-2, the majority of which is observed at a higher temperature. In the case of AgZr-1 on the other hand, removal of sulphur species occurs across a remarkably low temperature range. Two points should be noted: First, removal at this temperature is not consistent with the presence of zirconia sulphates [23], indicating either direct Ag-sulphate reduction or Ag-mediated reduction of support sulphates. Reduction of Ag-SO_4^{2-} (to SO_2) at lower temperature with respect to Al-SO_4^{2-} has been

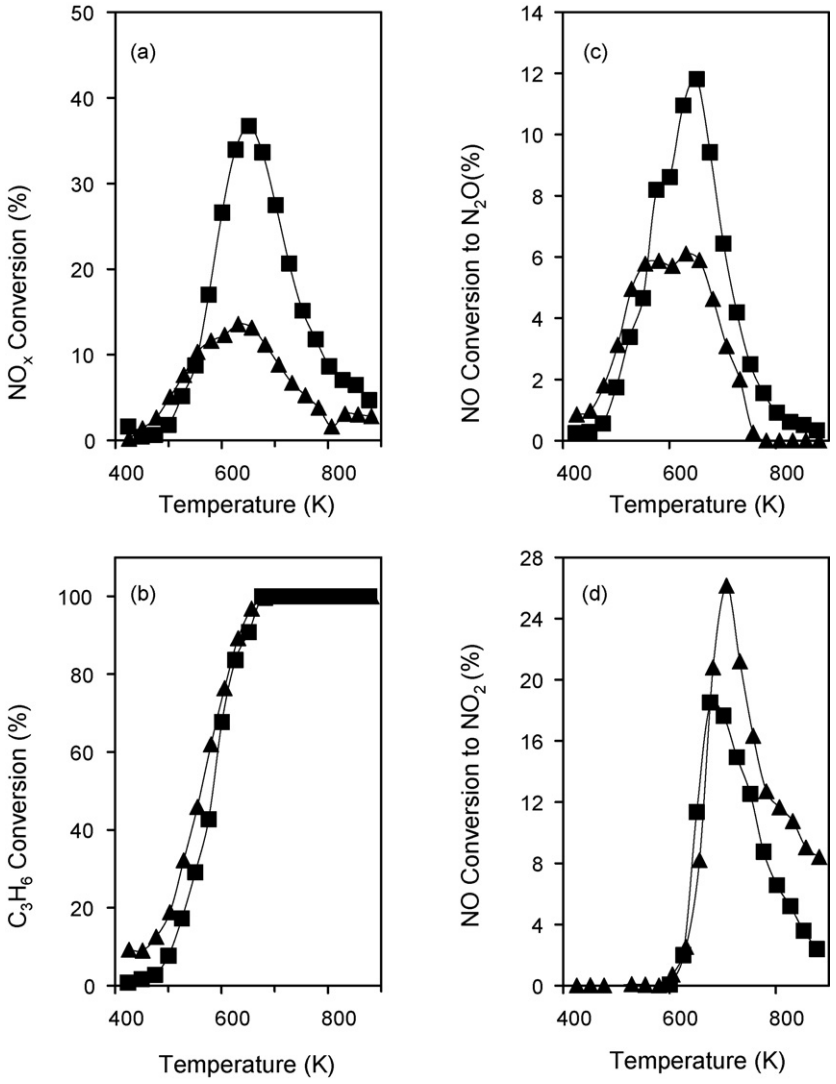

Fig. 5. Comparison of deNO_x activity of AgCe-1 (▲) and AgZr-1 (■) as a function of temperature: (a) NO_x (NO + NO_2) conversion, (b) C_3H_6 conversion, (c) NO conversion to N_2O, and (d) NO conversion to NO_2. 1000 ppm NO, C_3H_6, 5% O_2. W/F = 0.05 g s ml^{-1}.

reported, although the maximum reported here occurs at lower temperature (500 K vs 600–700 K) [24]. Second, sulphur is mainly removed as SO_2 (8.9 times the amount observed from AgAl-1/m^2) and not H_2S (1.8 times the amount observed from AgAl-1/m^2), suggesting that easily reduced sulphates predominate.

To further investigate the H_2 regeneration step, a variation of the TPR technique was employed, in which the samples were first exposed to a mixture of $SO_2 + O_2$ at 723 K before exposure to 5% H_2 at the same temperature, followed by TPR to 1073 K. The aim was to gain insight into removal of adsorbed SO_x species under isothermal conditions for subsequent *in situ* investigation (vide infra). The results are shown in Fig. 7. Consistently with Fig. 6, AgZr-1 shows mainly a very sharp SO_2 desorption peak during the isothermal step, with a relatively small H_2S signal. For AgCeZr-2 and AgAl-1 mixtures of SO_2 and H_2S are observed during the isothermal step, but in significantly smaller amounts. For AgCeZr-2 in fact, there is very little desorption. During the temperature ramped step, quite small signals are observed for AgZr-1 and AgAl-1, which indicates that the majority of the sulphur species have been removed at 723 K in the former case, and that the overall capacity is quite low in the latter. For AgCeZr-2 however, significant SO_2 and H_2S signals are observed, from which it can be concluded that the sulphur species are held too strongly to be removed at 723 K. Peak integration revealed that for AgZr-1 the total amounts of SO_2 and H_2S removed are, respectively, 26.3 and 2.1 times that observed from AgAl-1 (per m^2); while 2.9 times the amount of SO_2 and 2.5 times the amount of H_2S are observed for AgCeZr-2 with respect to AgAl-1.

3.3.2. *Activity test with in situ addition of SO_2 and regeneration of activity*

The effect of SO_2 on the deNO_x activity of AgAl-1, AgCeZr-2 and AgZr-1 was further investigated by means of isothermal tests at 723 K (Fig. 8). As noted above, at this temperature, all three catalysts show comparable activity (Figs. 3 and 4). The ability of H_2 (5%) to regenerate activity is also shown. For AgAl-1, as negligible quantities of NO_2 were formed, NO_x conversion also corresponds to NO conversion. All catalysts suffer from a significant deactivation when 50 ppm of SO_2 are added to the feed. However, there are a number of notable differences evident in the deactivation/regeneration behaviour:

(1) Deactivation of AgAl-1 begins immediately and is rapid. For AgCeZr-2 and, to a lesser extent, AgZr-1, a two-stage process is evident, in that a decrease in NO_2 production begins immediately, during which deNO_x activity remains high. Once NO_2

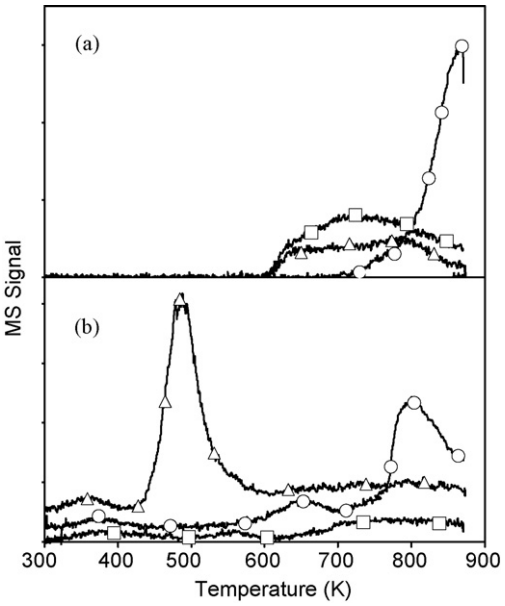

Fig. 6. Temperature programmed reduction profiles for AgAl-1 (□); AgCeZr-2 (○); and AgZr-1 (△) after prior exposure to SO_2 (300 ppm) + O_2 (5%): (a) m/e = 34 (H_2S); (b) m/e = 64 (SO_2). 5% H_2, 10 K min^{-1}. Sulphation: ramp to 873 K (10 K min^{-1}), held for 1 h and then cooled rapidly to ambient temperature in the SO_2 + O_2 mixture.

production stops, deNO_x activity begins to decrease. The two stages are more clearly delimited in the case of AgCeZr-2, by a brief period (20 min) where deNO_x activity remains almost constant after NO_2 production has ceased.

(2) Significant recovery of the deNO_x activity could be achieved in the case of zirconia-based materials by exposure to 5% H_2 at 723 K for 10 min, relatively mild regeneration conditions. In contrast, no significant regeneration of the AgAl-1 could be achieved under similar conditions or for reduction temperatures as high as 923 K (not shown).

(3) Under the deactivation/regeneration conditions used, NO_2 formation is irreversibly suppressed in the case of AgCeZr-2, whereas it is almost completely reversible in the case of AgZr-1.

The remarkable regeneration behaviour AgZr-1 was further investigated in a series of isothermal experiments conducted in an analogous manner as those in Fig. 8, but at lower temperatures (Fig. 9). It is clear from this figure that at lower temperature the behaviour of AgZr-1 begins to resemble that of AgCeZr-2. At all

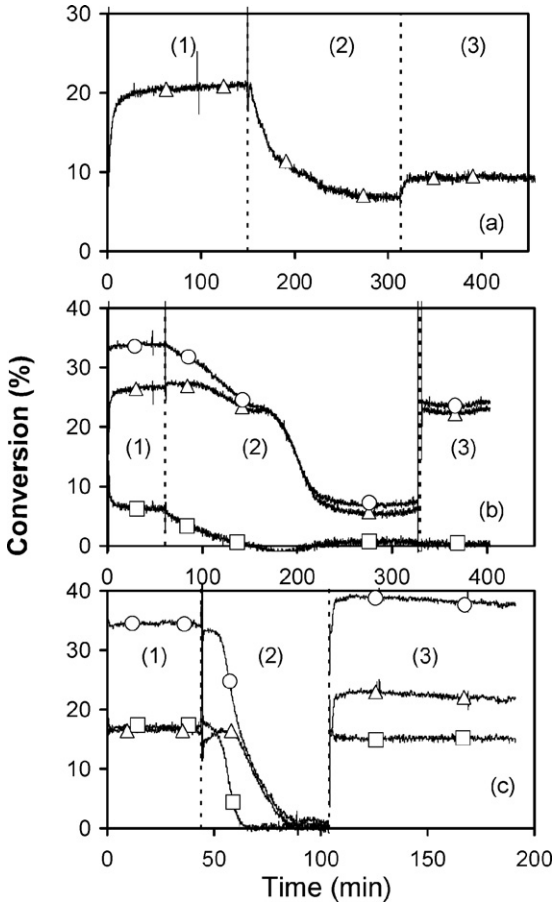

Fig. 8. deNO_x activity at 723 K over (a) AgAl-1, (b) AgCeZr-2 and (c) AgZr-1. (1) Activity in the absence of SO_2, (2) effect of SO_2 addition (50 ppm) to the feed, and (3) activity in the absence of SO_2 after reduction in H_2 (5% in He, 10 min) at 723 K. (○) Total NO conversion; (△) NO_x conversion to N_2 and N_2O (□) conversion of NO to NO_2. 1000 ppm NO, C_3H_6, 5% O_2; W/F = 0.05 g s ml^{-1}.

three temperatures shown, introduction of SO_2 to the feed results in immediate deactivation of the sample. At 673 K, the regeneration behaviour is similar to that of AgCeZr-2 at 723 K: deNO_x activity is recovered to a large extent by exposure to 5% H_2 for 10 min, while NO_2 formation remains completely suppressed. Treatment at 723 K results in more complete reactivation, similar to that shown in Fig. 8c. Investigation at 623 and 573 K reveal similar quantitative

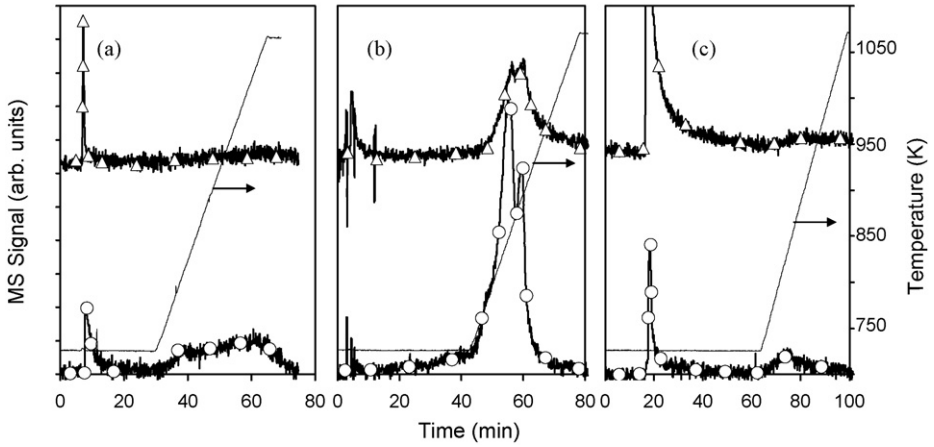

Fig. 7. Time-resolved signals for m/e = 34 (H_2S, ○) and m/e = 64 (SO_2, △) observed from (a) AgAl-1, (b) AgCeZr-2, and (c) AgZr-1 upon exposure to H_2 (5%) at 723 K, followed by ramping to 1073 K (10 K min^{-1}). The samples were first exposed to SO_2 (300 ppm) + O_2 (5%) at 723 K for 1 h.

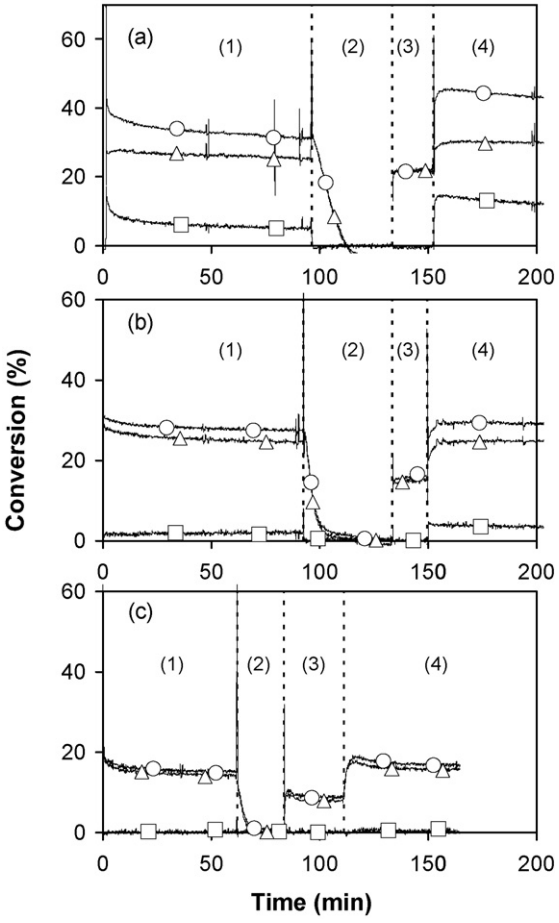

Fig. 9. DeNO$_x$ activity of AgZr-1 at (a) T = 673 K, (b) T = 623 K and (c) T = 573 K. (1) Activity in the absence of SO_2; (2) effect of SO_2 addition (50 ppm) to the feed; (3) activity in the absence of SO_2 after regeneration in H_2 (5% in He, 10 min) at the temperature of investigation; and (4) activity in the absence of SO_2 after reduction in H_2 (5% in He, 10 min) at 723 K. (○) Total NO conversion; (△) NO$_x$ conversion to N_2 and N_2O (□) conversion of NO to NO_2. 1000 ppm NO, C_3H_6, 5% O_2; W/F = 0.05 g s ml^{-1}.

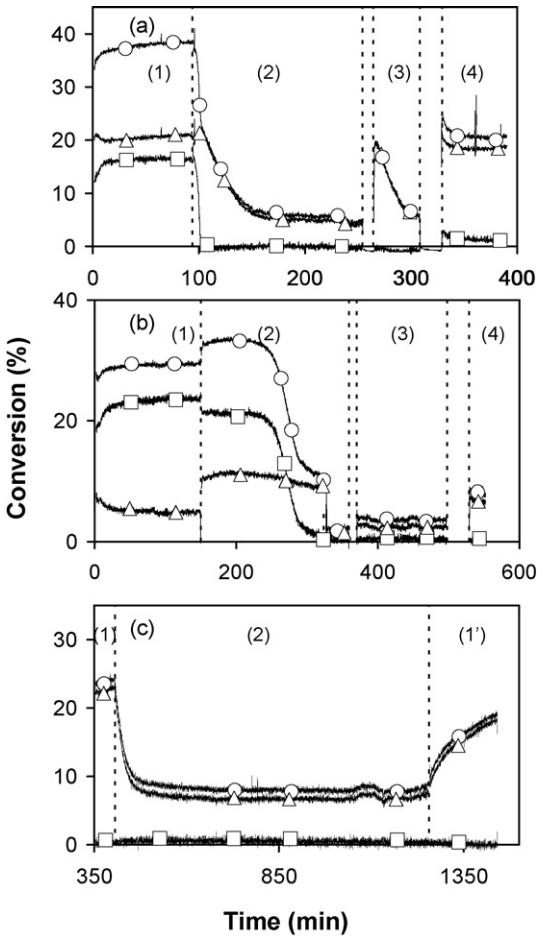

Fig. 10. (a) DeNO$_x$ activity at 723 K over AgZr-2: (1) activity in the absence of SO_2, (2) effect of SO_2 addition (50 ppm) to the feed, (3) activity in the presence of SO_2 after 10 min regeneration in H_2 (5%) at 723 K, (4) activity in the absence of SO_2 after 30 min regeneration in H_2 (5%) at 723 K. (b) DeNO$_x$ activity at 623 K over AgCe-1: (1), (2) as in (a), (3) activity in the absence of SO_2 after 10 min regeneration in H_2 (5%) at 723 K, (4) as in (a). (c) Effect of addition of SO_2 for a second time on activity of AgCeZr-2 at 723 K: (1) activity in the absence of SO_2 after 10 min regeneration in H_2 (5%) at 723 K; (2) effect of second SO_2 addition (50 ppm) to the feed; (1′) activity in the absence of SO_2. This was conducted immediately after the experiment shown in Fig. 8b. (○) total NO conversion; (△) NO$_x$ conversion to N_2 and N_2O (□) conversion of NO to NO_2. 1000 ppm NO, C_3H_6, 5% O_2; W/F = 0.05 g s ml^{-1}.

behaviour. However, after deactivation at these temperatures the effect of H_2 treatment at 723 K is not as efficient, especially in terms of regeneration of NO_2 formation, which could indicate a long-term deactivation effect.

Fig. 10 shows the results of a series of similar experiments over various catalysts, aimed at further clarifying the observations in Figs. 8 and 9. Fig. 10a shows the deactivation/regeneration behaviour of AgZr-2 at 723 K. This sample was prepared in order to ascertain whether the low surface area of the zirconia is a contributing factor in the behaviour exhibited by AgZr-1. There are two salient features which should be noted. The first is that, upon introduction of SO_2, the deactivation profile is similar to that of fresh AgZr-1 (Fig. 8a), but this sample maintains a higher residual activity after deactivation. The second is that the deNO$_x$ activity of this sample, but not its NO oxidation activity, is restored upon exposure to H_2. Thus, its behaviour is very similar to that of AgCeZr-2 in Fig. 8b. Upon reintroduction of the SO_2-containing feed, deactivation recommences immediately, while increasing the reduction time to 30 min resulted in marginal better recovery of NO oxidation activity. For the AgCe-1 sample (Fig. 10b), after introduction of SO_2 to the feed there is a relatively long period during which activity remains unaffected, after which NO oxidation activity decreases while deNO$_x$ activity remains largely unaffected and, finally, deNO$_x$ activity decreases. DeNO$_x$ activity only is restored by H_2 treatment, but the effect is rather small. Fig. 10c shows the response of AgCeZr-2 upon exposure to SO_2 for a second time, after the experiment shown in Fig. 8b. The sample deactivates immediately, in a manner very similar to that of AgAl-1 in Fig. 8a. After prolonged exposure, removal of SO_2 from the feed results in a slow but steady recovery of activity. Such behaviour was not noted for AgZr-1, as simply removing the SO_2 did not result in any recovery of activity. Indeed, when SO_2 was removed from the stream during the deactivation step of AgZr-1, i.e., at various stages before complete deactivation, no recovery was observed. Thus, it appears that H_2 is crucial to regenerate this sample.

3.3.3. *Activity tests after ex situ sulphur treatment*

An interesting aspect to emerge from the preceding sections is that the selectivity to N-containing products of extensively sulphated ceria–zirconia- and zirconia-supported Ag samples appears to be the same as that of aluminia-supported Ag. This was further investigated in a series of consecutive temperature programmed reaction tests over AgCeZr, performed after various treatments (Fig. 11). The fresh catalyst shows desorption of NO$_x$ (both NO and NO_2) at low temperature followed by NO$_x$ conversion at higher temperature. Above 673 K, after NO$_x$ conversion has gone through

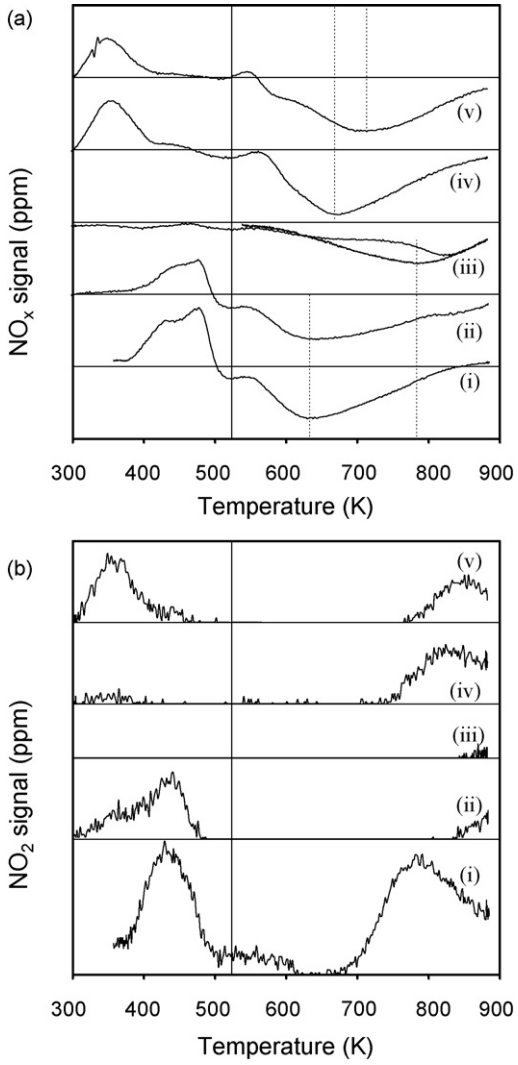

Fig. 11. (a) NO_x and (b) NO_2 signals observed during consecutive temperature programmed reaction over AgCeZr-2 after various treatments: (i) fresh catalyst; (ii) after 1 h *ex situ* treatment in SO_2 (50 ppm) + 5% O_2 at 723 K; (iii) after ramping from room temperature to 723 K in SO_2 (50 ppm) + 5% O_2, holding for 1 h and cooling in the same mixture; (iv) after ramping from room temperature to 723 K in 5% H_2, holding 10 min and cooling to room temperature; (v) after the same treatment as in (iv). 1000 ppm NO, C_3H_6, 5% O_2; W/F = 0.05 g s ml^{-1}.

its maximum, NO_2 formation is observed (profile i). Exposure to SO_2 at 723 K for 1 h has little effect on the NO_x conversion (profile ii), which might be taken to indicate that the sample is resistant to SO_x poisoning. However, differences are observed in the desorption profile, which is suppressed and appears more broad; and in the suppression of NO_2 formation at high temperature. A more severe SO_x treatment strongly deactivates the sample (profile iii): the maximum of deNO_x activity is at ca 773 K, close to that of the Ag/Al_2O_3 samples in Fig. 3, and high temperature NO_2 formation is completely suppressed. Thus, the high activity after the previous treatment is most likely due incomplete or partial coverage, which strongly affects NO_2 formation but only mildly the deNO_x activity. Relatively mild regeneration (10 min at 723 K) results in recovery of deNO_x activity (profile iv), but with a maximum at a slightly higher temperature with respect to the fresh material. NO_2 production above 723 K also reappears. However, the NO_x desorption at low temperature does not contain NO_2 and is observed at lower temperature. Finally, a second reduction treatment results in somewhat lower deNO_x activity with a maximum at higher temperature (profile v), while NO_2 production reappears at low temperature. The

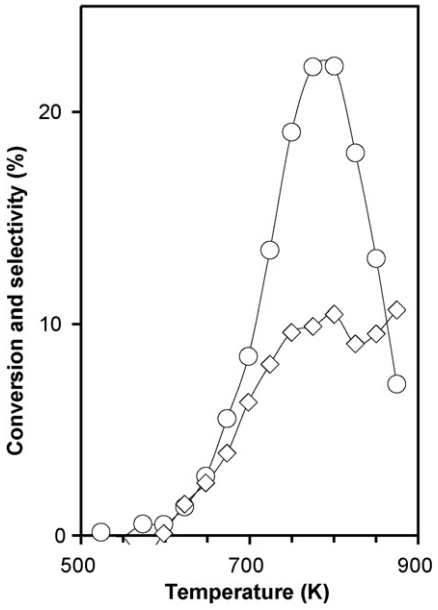

Fig. 12. NO_x conversion (○) and selectivity to CO (◊) over sulphated AgCeZr-2. 1000 ppm NO, C_3H_6, 5% O_2; W/F = 0.05 g s ml^{-1}. Sulphation conditions: 50 ppm SO_2, 5% O_2, ramp to 873 10 K min^{-1}, hold 1 h, cool-down.

initial profile of the fresh catalyst is not recovered, indicating irreversible surface changes, which may be due to difficult-to-remove sulphur.

On the basis of these observations, a full activity test was also performed over AgCeZr-2 after a very severe *ex situ* sulphation procedure, similar to those before the TPR profiles (Fig. 7). Not only was the shift in activity range to high temperature confirmed, but formation of CO was also observed. Thus, the sulphated AgCeZr-2 sample exhibits the same characteristics as AgAl-1 (Fig. 12).

3.4. Effect of H_2O and $H_2O + SO_2$ on the SCR of NO with C_3H_6

The effect of H_2O (10%) and H_2O (10%) + SO_2 (50 ppm) on the activity at 723 K were compared for AgCeZr-2, AgZr-1 and AgAl-1. The results are summarised in Fig. 13. On addition of H_2O to the feed (Fig. 13a), both zirconia-containing catalysts show a decrease in NO_x conversion. However, the suppression observed in the case of AgCeZr-2 is smaller, thereby indicating a better resistance to the effect of H_2O. On removal of water, the recovery observed is more complete in the case of AgZr-1. With regard to C_3H_6 conversion, conversion remains at 100% for AgCeZr-2 throughout the set of experiments. For AgZr-1, there is a slight decrease in C_3H_6 conversion upon addition of H_2O and a recovery upon its removal. These changes can be considered to be negligible. For AgAl-1, the presence of H_2O at 723 K almost completely suppressed activity: deNO_x activity decreases from 26% to <5%. Activity was recovered once H_2O was removed from the feed (HC, 3% lower, deNO_x 2% higher).

Fig. 13b summarises the effect of the presence of $H_2O + SO_2$ on the three catalysts at 723 K. In these experiments H_2O was added first, followed by SO_2 after stabilisation of the conversion. Catalyst regeneration at 723 K was also performed (5% H_2, 10 min) after deactivation. For the zirconia-containing samples both deNO_x activity and C_3H_6 conversion are strongly suppressed, but activity is largely recovered on reduction of the samples. In the case of AgAl-1, two salient points emerge. The first is that NO_x conversion is higher in the simultaneous presence of H_2O and SO_2 than in the presence of H_2O only (10% vs 4%). This observation is in line with that of Miyadera and Yoshida [1]. C_3H_6 conversion, on the other

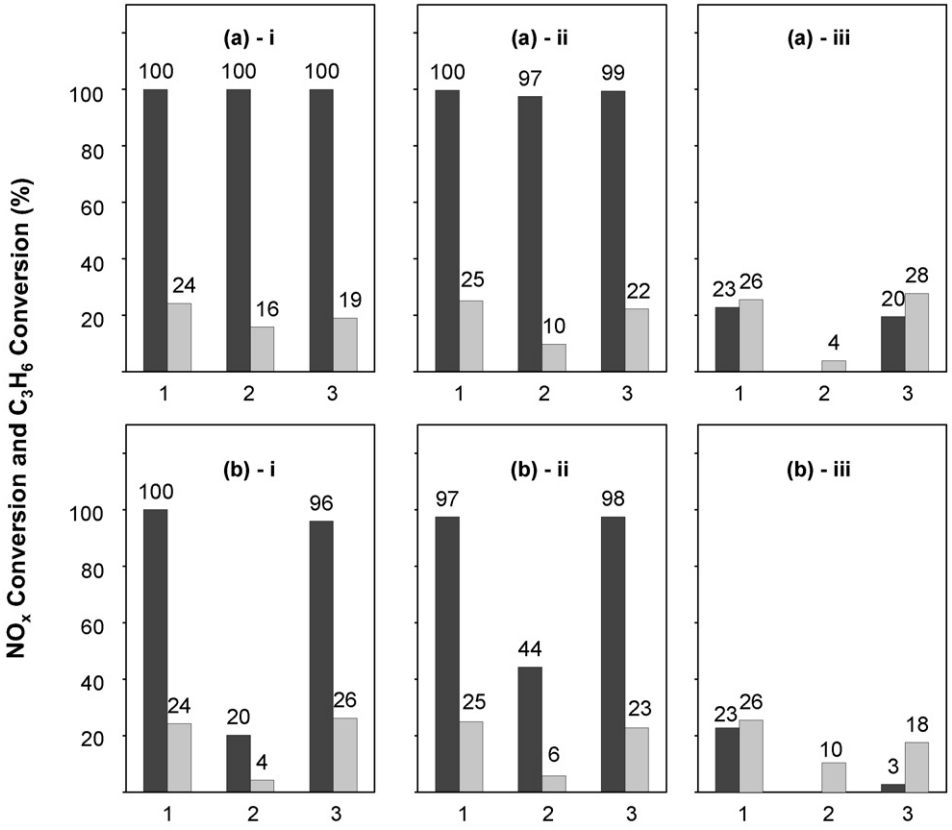

Fig. 13. (a) Effect of H_2O on C_3H_6 conversion (dark grey) and deNO_x activity (light grey) at 723 K. (i) AgCeZr-2; (ii) AgZr-1 and (iii) AgAl-1. (1) before H_2O; (2) with H_2O; (3) after H_2O. 1000 ppm NO, C_3H_6, 5% O_2, (10% H_2O). W/F = 0.05 g s ml^{-1}. (b) Effect of $H_2O + SO_2$ on C_3H_6 conversion (dark grey) and deNO_x activity (light grey) at 723 K and efficiency of regeneration at 723 K. (i) AgCeZr-2; (ii) AgZr-1 and (iii) AgAl-1. (1) Before $H_2O + SO_2$; (2) with $H_2O + SO_2$; (3) without $SO_2 + H_2O$ after treatment with H_2 (5%) at 723 K (10 min). 1000 ppm NO, C_3H_6, 5% O_2, (10% H_2O, 50 ppm SO_2). W/F = 0.05 g s ml^{-1}. All conversions shown are those obtained once stable responses were observed.

hand, is completely suppressed. The second noteworthy feature is that after regeneration there is significant recovery of activity (from 10% to 18%). The presence of water vapour may therefore stabilise the activity of Ag/Al_2O_3 by removing sulphur from the surface. However, some accumulation of SO_2 may be inferred from the observation that deNO_x activity is not completely recovered, while C_3H_6 conversion remains suppressed.

4. Discussion

4.1. Effect of Ag particle size on activity range

The present data indicate that the range of temperature across which the deNO_x activity is observed for AgCeZr-1, AgCeZr-2, AgZr-1 (and AgCe-1) is lower than that observed for the Ag/Al_2O_3 catalysts. As indicated in the introduction, shifts in activity to low temperature over Ag/Al_2O_3 have been interpreted in terms of a change in mechanism due to the presence of the large Ag particles. The TEM data *do not support* this explanation for the present alumina-free Ag samples. On the contrary, the data indicates significant variations in the Ag particle size distribution across the samples investigated (compare AgZr-1, AgCeZr-1 and AgCeZr-2), *yet variation in the temperature range of activity was not observed*. Clearly, the TEM data only indicate the dispersions of the starting materials and not under SCR reaction conditions. However, while the mobility of silver species during the SCR reaction is well accepted [3,25,26] it is unlikely that similar dispersions could result under our reaction conditions. Furthermore, in comparison to AgZr-1, smaller (and similar) amounts of NO_2 are formed over AgCeZr-1 and AgCeZr-2, despite the fact that they show smaller and bigger particles, respectively. In fact, the amount of NO_2 formed is low with respect to that previously observed with high Ag loadings. To further test this hypothesis a 10% $Ag/Ce_{0.2}Zr_{0.8}O_2$ was prepared and tested under identical reaction conditions. The sample showed activity in the same range (T_{max} NO_x = 653 K), but with very high selectivity to NO oxidation (32% at 653 K) and, consequently, relatively low deNO_x activity (16% at 653 K).

Clearly, the silver particle size is an important consideration in the deNO_x activity. Much attention has been devoted to ascertaining the nature of the active Ag species in Ag/Al_2O_3, with conflicting conclusions. Thus, nano-Ag particles, Ag clusters, nano-sized Ag_2O clusters, both Ag^+ and Ag particles, and β silver aluminate-like species have all been suggested to be the active species [3]. Shimizu and Satsuma have suggested that the nature of the active Ag species depends on the hydrocarbon used [3], while Burch has attributed this scatter of interpretation to the wide-spread use of *in situ* DRUV–vis and the uncertain interpretation of these spectra [2]. The optimal loading has been linked either to an optimal particle size or an optimal balance between dispersed Ag^+ and $Ag_m^{\delta+}$ clusters, and many reports have indicated that atomically dispersed Ag^+ species alone show low activity. In fact, our data is consistent with this observation, as Table 3 indicates that very high dispersion does not favour deNO_x activity. On the other hand, as discussed above, deNO_x activity is not favoured by high Ag loading. Thus, in line with the literature reports for Ag/Al_2O_3, our data indicates that activity is not favoured when the Ag particle is either too big or too small also for our Al_2O_3-free samples.

The data obtained for present Ag/Al_2O_3 samples are quite illustrative from the point-of-view of the effect of the silver particle size. The presence of the bimodal particle size distribution for AgAl-1 neatly explains the unusual "plateau" in the C_3H_6 conversion to CO_2. This is consistent with the observations that large Ag particles

promote unselective combustion at lower temperatures [6], at the expense of deNO$_x$ activity, and is in line with the lower NO$_x$ conversion for this sample compared with AgAl-2. The absence of NO$_2$ and N$_2$O, which are normally observed over highly loaded Ag/Al$_2$O$_3$ catalysts [6], may be attributed to the small number of these particles. The majority of the particles in AgAl-2 are smaller than 20 nm and this sample exhibits the expected behaviour of "dispersed" Ag/Al$_2$O$_3$ catalysts with low Ag loadings. We therefore conclude that the variations in maximum NO$_x$ for same-support samples may be reasonably attributed to differences in Ag dispersion, but the shift in activity range observed over the CeO$_2$–ZrO$_2$ and ZrO$_2$ samples is due to the use of the different supports.

4.2. Effect of the support on the activity of Ag

Investigations of catalysts with similar loadings have shown that the mechanism of deNO$_x$ over Ag/Al$_2$O$_3$ samples is rather complex, consisting of a number of parallel reactions. However, the majority of investigations retain that both Ag and alumina are directly involved in the mechanism. Indeed, with regard to the role of the support, even the source of the Al$_2$O$_3$ used in the preparation [27] or the physical characteristics of the alumina have been reported to affect the activity observed [28]. In addition, there have been a number of reports which indicate that modification of the Al$_2$O$_3$ support can enhance either the activity or the sulphur tolerance of Ag/Al$_2$O$_3$ catalysts. Thus, inclusion of Mg, TiO$_2$ and SiO$_2$ have been reported to improve various aspects of the C$_3$H$_6$-SCR activity behaviour [29–31]. Here, in an analogous manner, we investigate the effect of changing the support on the C$_3$H$_6$-SCR activity for a series of 2 wt% Ag samples.

An important indication on the role of the support is provided by the CO formation behaviour. CO formation is a feature of alumina-supported Ag deNO$_x$ catalysts [1,8,16]. Yields up to 40% of CO have been reported [32], whereas when NO$_2$ was reduced instead of NO over acidic silver-containing zeolites, a stoichiometry of 1 CO molecule per N$_2$ molecule formed was obtained [33]. The relatively poor oxidation capability of silver might account for this observation. However, a more plausible explanation may be found in the observation that decomposition of surface intermediates formed in the NO/O$_2$/C$_3$H$_6$ reaction over Ag/Al$_2$O$_3$ produces considerable amounts of CO along with N$_2$ and CO$_2$ [34]. Consistently, we observe that the appearance of CO coincides with the deNO$_x$ reaction. Similarly, while the absence of CO over the CeO$_2$-containing catalyst might be expected on the basis that ceria can efficiently catalyse hydrocarbon combustion [35], ZrO$_2$ is not considered to be effective for catalytic oxidation [6]. Accordingly, the absence of CO in the reaction products over AgZr-1 might be attributed to a co-operative effect of the Ag/ZrO$_2$ system, or to gas reaction after the catalyst (vide infra), and indicates the crucial role of these supports in modifying the catalytic activity of the supported silver with respect to Ag/Al$_2$O$_3$.

It should be noted that a contribution of homogeneous reaction of desorbed intermediates to the lean-deNO$_x$ activity of Ag/Al$_2$O$_3$ has been demonstrated by Eranen et al. [36] We tested this possibility and found that placing a 1% Pt/Al$_2$O$_3$ catalyst immediately after AgCeZr-2 resulted in a decrease of the deNO$_x$ activity observed for the combined system across the temperature range where AgCeZr-2 alone is active. This is illustrated in Fig. 14. This observation is consistent with the observations of Eranen et al. The results reported on the effect of W/F are also compatible with possible occurrence of homogeneous reactions, as, in that case, the temperature range of activity should depend on desorption of intermediates from the catalyst, whereas the extent of conversion achieved should depend on the space velocity. Clearly, the desorption behaviour of reaction intermediates formed at the surface is strongly dependent on the nature of the support.

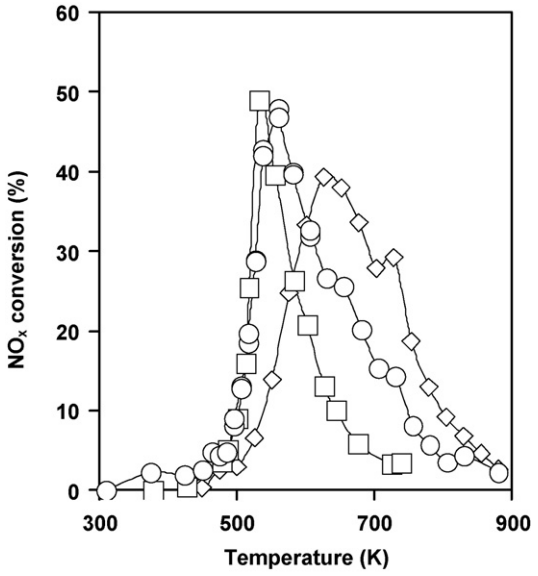

Fig. 14. NO$_x$ conversion over AgCeZr-2 (◊); 1% Pt/Al$_2$O$_3$ (□) and AgCeZr-2 + 1% Pt/Al$_2$O$_3$ (○). 50 mg aliquots of each catalyst were used. 1000 ppm NO, C$_3$H$_6$, 5% O$_2$. Flow rate = 60 ml min^{-1}.

The investigations conducted using SO$_2$ offer important insights from the point-of-view of the involvement of the support. Overall, the inhibiting effect of SO$_2$ is attributed to the retention of SO$_x$ species on the surface and the regeneration behaviour to their removal. Consistently, minimal time-on-stream deactivation was observed on a similar time scale in the absence of SO$_2$. It should be noted that previous reports have indicated that *ex situ* approaches may not represent the true uptake of SO$_x$ under reaction conditions [10,37]. Increased *in situ* sulphur uptake compared to *ex situ* was reported, which should contribute to more rapid deactivation. This cannot be excluded in the present results.

The TPR results indicate that the AgZr-1 and AgCeZr-1 have higher overall normalised capacities for sulphur storage with respect to AgAl-1, with the capacity of AgZr-1 being the highest of the three. However, there is not a direct correlation between SO$_x$ capacity and deactivation or between SO$_x$ removal and regeneration. The overall behaviour observed can be best understood in terms of selective poisoning and regeneration of specific sites.

The alumina-based material begin to deactivate immediately upon introduction of SO$_2$ (Fig. 8). Thus, sites necessary for deNO$_x$ activity are immediately blocked. It is likely that such sites include the Ag particles. The behaviour in Fig. 7 suggests that, for Ag/Al$_2$O$_3$, the high initial isothermal activity described depends on a limited number of sites which retain SO$_2$ strongly (high temperature peaks), and not on those sites from which they are more easily removed (isothermal peaks). Alternatively, both may be necessary.

For AgCeZr-2, AgZr-1 (Fig. 8) and AgZr-2 (Fig. 10), the deactivation is a two-stage procedure. During the first stage, deNO$_x$ activity remains high while NO$_2$ production decreases immediately. This may be explained by an initial selective poisoning of support sites by SO$_x$ retention. The relatively high levels of NO$_x$ conversion maintained suggest that these support sites are largely responsible for NO$_2$ production. Evidence for this hypothesis is also found in Fig. 11, in which a relatively limited exposure to SO$_2$ suppresses NO$_2$ formation while NO$_x$ conversion is maintained; while after a longer exposure both NO$_x$ conversion and NO$_2$ formation are suppressed. The decrease in deNO$_x$ activity once NO$_2$ production ceases (stage 2) can be interpreted in terms of a saturation effect. Once these support sites have been blocked, further adsorption, most likely on Ag, rapidly deactivates the sample. The more brief first stage in the case

of both ZrO_2-containing materials investigated (Figs. 8 and 10) may be attributed to a poor ability for this support to scavenge the poisoning sulphur from the metal. We believe that this characteristic is introduced or enhanced by the presence of ceria, as indicated by the relatively long period of resistance to poisoning for the AgCe-1 sample (Fig. 10). Thus, SO_2 oxidation at the metal followed by migration to the support sites may allow a period of resistance to poisoning of $deNO_x$ activity [9]. In the case of the AgCeZr-2 sample, the observation that $deNO_x$ activity remains high while NO_2 production decrease, combined with the observation that there is significant $deNO_x$ activity across a much lower temperature range that that in which there is direct NO oxidation activity (Fig. 4), is worthy of note. These observations are consistent with reports that claim that NO oxidation to NO_2 is not important in the mechanism of efficient C_3H_6-SCR over Ag/Al_2O_3 and that a more complex mechanism operates [13]. On the other hand, there is a high temperature shoulder in the C_3H_6–SCR $deNO_x$ activity which coincides with the maximum of NO oxidation activity in the absence of C_3H_6. A possible interpretation is that there is a change in mechanism with temperature. However, more detailed mechanistic investigation would be needed to clarify this point.

Upon treatment in H_2 at 723 K, only for AgZr-1 are most of the adsorbed sulphur species removed (Fig. 7), but in no case is complete removal effected. The observed differences in activity and/or selectivity after reduction may be attributed to the presence of retained sulphur species. The regeneration conditions are somewhat mild to induce changes such as sintering, which might otherwise be held responsible. The majority of SO_x retained on AgCeZr-2 is not removed by H_2 (Fig. 7). However the small amount removed restores the activity to the point where NO_2 production had previously ceased (Fig. 8). Upon subsequent exposure to SO_2 (Fig. 10c), the presence of retained sulphur species largely eliminate the previously observed resistance to SO_2 and deactivation takes place in a manner qualitatively similarly to that observed in the second stage and for the other samples, i.e., rapid and immediate. Thus, regeneration of $deNO_x$ activity for this sample appears to depend on a limited number of sites from which sulphur species are more easily removed. Similar behaviour for Ag/Al_2O_3, at a much higher reduction temperature, has been attributed to Ag sites [38].

Fig. 8 indicates pronounced differences between the ZrO_2- and $Ce_{0.16}Zr_{0.84}O_2$-supported samples. However, further investigation evidenced a general convergence of behaviour. Lowering the temperature of the isothermal deactivation/regeneration tests results in the AgZr-1 material exhibiting rather similar regeneration behaviour to AgCeZr-2 (Fig. 9). This may be attributed to a less efficient removal of adsorbed species at lower temperature. At 723 K, the AgZr-2 sample exhibits similar regeneration behaviour to that of AgCeZr-2 (Fig. 10a). Thus, we feel that the most likely explanation of the remarkable regeneration behaviour of AgZr-1 is the relatively high ratio of exposed metal surface area to total surface area evidenced by the TEM data. As noted above, the temperature at which SO_2 is observed for AgZr-1 during TPR is not consistent with reduction of sulphated zirconia alone [23] and we attribute the observation to reduction of Ag-sulphates or Ag-mediated sulphate removal. The observation indicates that that the metal can exert a more extensive influence over the desorption behaviour for this sample.

The importance of the acid–base properties of the support in controlling the $deNO_x$ activity Ag-based catalysts is well established [3] and the deactivation and regeneration behaviour could also be linked to these properties. In this context, it is significant to note that *ex situ* sulphated AgCeZr-2 shows activity similar to AgAl-1 (Figs. 11 and 12), given that sulphation of CeO_2–ZrO_2 is known to increase the strength of surface acid sites of the mixed oxide [39].

In the presence of H_2O, all three samples investigated indicate a suppression of activity which is reversed once H_2O is removed. Both zirconia-containing samples show better resistance to H_2O in comparison with Ag/Al_2O_3, for which the data is consistent with a competitive adsorption mechanism. In the simultaneous presence of H_2O and SO_2, all three samples deactivate. For AgAl-1 the negative effects of SO_2 are somewhat offset by H_2O and the regeneration of $deNO_x$ activity observed is improved; while for the zirconia-containing materials, complete regeneration of activity is observed.

5. Conclusions

The comparison of $deNO_x$ activity over 2 wt% loaded Ag catalysts clearly showed that the range of temperature where $deNO_x$ activity is observed is strongly influenced by the nature of the support; CeO_2- and ZrO_2-based catalysts show a large shift of the range of activity towards low temperatures compared to Al_2O_3-based catalysts. *Ex situ* characterisation of the catalysts indicates that this effect is not associated with Ag particle size. Thus, our work suggests that the activity temperature range of supported Ag materials for lean $deNO_x$ can be tuned by appropriate choice of the support materials. Further, the change of the support completely suppresses the undesirable formation of CO as a product of reaction.

The use of ZrO_2-based supports improves both the SO_x resistance and the ease of regeneration of the Ag-based catalysts. Finally, inclusion of ceria in the ZrO_2-based support formulation favours the SO_x resistance behaviour as ceria seems to act as a sulphur scavenger. This results could be of interest also for the development of efficient sulphur traps for the so-called NSR (NO_x storage/release) catalysts [2].

Acknowledgements

The University of Trieste and the INCA Consortium – Progetto ECOMOS-FIRB (DM26133) are gratefully acknowledged for financial support. M.B. is recipient of a post-doc grant form Università di Torino – Regione Piemonte (Assegno Azione C). The authors are grateful to Prof. S. Coluccia (University of Torino) and Prof. M. Rossi (University of Milan) for helpful discussions. Mr. E. Merlach (University of Trieste) is gratefully acknowledged for technical collaboration.

References

[1] T. Miyadera, K. Yoshida, Chem. Lett. (1993) 1483–1486.
[2] R. Burch, Catal. Rev. Sci. Eng. 46 (2004) 271–333.
[3] K.I. Shimizu, A. Satsuma, Phys. Chem. Chem. Phys. 8 (2006) 2677–2695.
[4] H. He, X. Zhang, Q. Wu, C. Zhang, Y. Yu, Catal. Surv. Asia 12 (2008) 38–55.
[5] S. Roy, M.S. Hegde, G. Madras, Appl. Energy 86 (2009) 2283–2297.
[6] K.A. Bethke, H.H. Kung, J. Catal. 172 (1997) 93–102.
[7] F.C. Meunier, R. Ukropec, C. Stapleton, J.R.H. Ross, Appl. Catal. B 30 (2001) 163–172.
[8] M. Haneda, Y. Kintaichi, M. Inaba, H. Hamada, Bull. Chem. Soc. Jpn. 70 (1997) 499–508.
[9] N. Hickey, P. Fornasiero, J. Kaspar, M. Graziani, G. Martra, S. Coluccia, S. Biella, L. Prati, M. Rossi, J. Catal. 209 (2002) 271–274.
[10] T.N. Angelidis, N. Kruse, Appl. Catal. B 34 (2001) 201–212.
[11] P.W. Park, C.L. Boyer, Appl. Catal. B 59 (2005) 27–34.
[12] S. Satokawa, K. Yamaseki, H. Uchida, Appl. Catal. B 34 (2001) 299–306.
[13] F.C. Meunier, V. Zuzaniuk, J.P. Breen, M. Olsson, J.R.H. Ross, Catal. Today 59 (2000) 287–304.
[14] E. Seker, J. Cavataio, E. Gulari, P. Lorpongpaiboon, S. Osuwan, Appl. Catal. A 183 (1999) 121–134.
[15] R. Burch, J.P. Breen, F.C. Meunier, Appl. Catal. B 39 (2002) 283–303.
[16] K.I. Shimizu, A. Satsuma, T. Hattori, Appl. Catal. B 25 (2000) 239–247.
[17] R. Di Monte, P. Fornasiero, S. Desinan, J. Kaspar, J.M. Gatica, J.J. Calvino, E. Fonda, Chem. Mater. 16 (2004) 4273–4285.
[18] C. de Leitenburg, A. Trovarelli, J. Llorca, F. Cavani, G. Bini, Appl. Catal. A 139 (1996) 161–173.
[19] F. Porta, L. Prati, M. Rossi, S. Coluccia, G. Martra, Catal. Today 61 (2000) 165–172.
[20] J. Kaspar, P. Fornasiero, N. Hickey, Catal. Today 77 (2003) 419–449.
[21] E. Seker, E. Gulari, J. Catal. 179 (1998) 339–342.
[22] J.B. Laizet, A.K. Soiland, J. Leglise, J.C. Duchet, Top. Catal. 10 (2000) 89–97.
[23] M. Waqif, O. Saur, J.C. Lavalley, Y. Wang, B.A. Morrow, Appl. Catal. 71 (1991) 319–331.

[24] K. Shimizu, T. Higashimata, M. Tsuzuki, A. Satsuma, J. Catal. 239 (2006) 117–124.
[25] J.P. Breen, R. Burch, C. Hardacre, C.J. Hill, J. Phys. Chem. B 109 (2005) 4805–4807.
[26] S. Pal, G. De, Mater. Res. Bull. 44 (2009) 355–359.
[27] R. Zhang, S. Kaliaguine, Appl. Catal. B Environ. 78 (2008) 275–287.
[28] H.W. Jen, Catal. Today 42 (1998) 37–44.
[29] P.A. Kumar, M.P. Reddy, B. Hyun-Sook, H.H. Phil, Catal. Lett. (2009).
[30] N. Jagtap, S.B. Umbarkar, P. Miquel, P. Granger, M.K. Dongare, Appl. Catal. B Environ. 90 (2009) 416–425.
[31] J. Li, Y. Zhu, R. Ke, J. Hao, Appl. Catal. B Environ. 80 (2008) 202–213.
[32] A. MartinezArias, M. FernandezGarcia, A. IglesiasJuez, J.A. Anderson, J.C. Conesa, J. Soria, Appl. Catal. B 28 (2000) 29–41.
[33] J.A. Martens, A. Cauvel, A. Francis, C. Hermans, F. Jayat, M. Remy, M. Keung, J. Lievens, P.A. Jacobs, Angew. Chem. Int. Ed. 37 (1998) 1901–1903.
[34] S. Sumiya, M. Saito, H. He, Q.C. Feng, N. Takezawa, K. Yoshida, Catal. Lett. 50 (1998) 87–91.
[35] A. Trovarelli, Catal. Rev. Sci. Eng. 38 (1996) 439–520.
[36] K. Eranen, L.E. Lindfors, F. Klingstedt, D.Yu. Murzin, J. Catal. 219 (2003) 25–40.
[37] A. Abe, N. Aoyama, S. Sumiya, N. Kakuta, K. Yoshida, React. Kinet. Catal. Lett. 65 (1998) 139–144.
[38] F.C. Meunier, J.R.H. Ross, Appl. Catal. B 24 (2000) 23–32.
[39] B.M. Reddy, P.M. Sreekanth, P. Lakshmanan, A. Khan, J. Mol. Catal. A: Chem. 244 (2006) 1–7.